Hindawi
Mathematical Problems in Engineering
Volume 2022, Article ID 8467627, 12 pages
https://doi.org/10.1155/2022/8467627

Research Article

Research on Lane Change Motion Planning Steering Input Based on Optimal Control Theory

Yongsheng Liu and Yingjie Liu

School of Mechanical and Automation, Weifang University, Weifang 261061, Shandong, China

Correspondence should be addressed to Yingjie Liu; ufoliuyingjie@163.com

Received 23 April 2022; Revised 28 May 2022; Accepted 30 May 2022; Published 16 June 2022

Academic Editor: Jie Hu

Aiming at traditional control methods are not suitable for solving the multiconstraint problem of the vehicle steering and lane-change maneuvering process, a hybrid optimization scheme based on dynamic adaptive salp swarm algorithm and Gaussian pseudospectral method (DASSA-GPM) is proposed for its strong global search capability. Based on a steering inverse dynamics model, the lane change motion planning steering problem is converted into an optimal control problem which is then converted into a nonlinear programming problem by applying the adaptive salp group algorithm which is solved through the sequential quadratic programming (SQP) method finally. The simulation results verify the effectiveness and feasibility of the proposed dynamic adaptive salp swarm algorithm and hybrid optimization scheme. In addition, compared with GPM which the absolute error of steering wheel angle is 8.2×10^{-4} degree, the proposed method has higher computational accuracy, which absolute error of steering wheel angle is 5.5×10^{-4} degree. At the same time, under the same calculation accuracy (10^{-3}), compared with GPM which CPU time is 4.81 s, the proposed method has higher calculation efficiency which CPU time is 3.86 s when solving non-smooth problems. The proposed method can provide a reference value into the active safety of manned and unmanned vehicles.

1. Introduction

Unreasonable lane change will cause traffic jams in traffic, affect travel time, and cause indirect losses to economic properties. If the intelligent assistance system detects danger earlier than the driver, it can provide early warning within the effective time or take over the driving control through the controller to reduce the probability of accidents [1]. Therefore, people use active safety systems as a measure to reduce the incidence of traffic accidents. Among them, the obstacle avoidance assist system based on braking is widely used. At present, people are also committed to study the technology of automatic obstacle avoidance through braking and steering, and change lanes as well as solving the inverse dynamics of vehicle lane change manipulation. Lane change behavior is one of the factors that affects the safety of vehicles. Relevant studies have shown that lane change will increase the probability of traffic conflict points and even cause traffic accidents of different degrees. Lane change is one of the most common and dangerous driving behaviors during vehicle driving. This behavior requires real-time driving behavior decision-making and vehicle motion control based on road environment information. At the same time, it is also necessary to consider the impact of the speed, ride comfort, and safety on passengers during the lane change process. Therefore, the study of lane change motion planning behavior has become a difficult and hot spot in the field of vehicle driving gradually. Among them, how to quickly and accurately plan lane change paths and effectively track the desired path is the basis for the realization of the vehicle lane change function. It is also one of the key technologies to improve the active safety of vehicles [2, 3]. In summary, the research on the characteristics of the dangerous driving behavior of vehicles in lane change can understand the mechanism of lane change risk and objectively analyze the possible risks of lane change from multiple perspectives such as the lateral stability of the vehicle and the avoidance of collisions between vehicles. The discrimination

results can provide references for the establishment and verification of vehicle lane-changing warning models. By identifying the driver's lane change intention, it provides a starting point for the early warning system to start predicting and then establishes lane-changing early warning rules on the premise of avoiding collisions between lane-changing vehicles and surrounding vehicles, which can help drivers avoid risks and make correct decisions, reducing traffic accidents caused by lane-changing behaviors, and improving road capacity. Overtaking in the process of high-speed driving is a common driving behavior, and automatic overtaking is not only related to path planning and speed control but also the safety of high-speed driving cannot be ignored, especially on low adhesion roads where the vehicle is more prone to instability. Therefore, the coordinated control between trajectory tracking accuracy and lateral stability must be considered. To ensure that the vehicle can achieve overtaking efficiently and safely, three key problems must be resolved: planning the overtaking path and driving speed reasonably; realizing accurate tracking of trajectory; ensuring the safety and comfort of the vehicle during overtaking.

Vehicle lane change path planning with high-speed is an important part of unmanned technology and also an important basis for using unmanned technology to reduce high-speed traffic accidents. Therefore, it is meaningful work to deeply study the path planning method for vehicle high-speed lane change motion planning avoidance. Based on the analysis of the vehicle lane-changing process, the vehicle lane-changing decision-making behavior is analyzed based on the actual road traffic vehicle conditions. When the lane-changing vehicle fails to meet the driver's expectation or the preceding vehicle brakes, the driver will first judge the distance between the vehicle and the preceding vehicle. When the distance is small, the driver chooses emergency braking to increase the safety distance. When the appropriate safety distance is reached, the driver determines whether the requirements for changing lanes are met by judging the motion information of the vehicles in the adjacent lanes, as well as the distance between the vehicle and the preceding and following vehicles in the adjacent lanes.

The problem of vehicle lane change motion planning has been widely studied. A brief review is presented in the following.

Xu et al. [3]. proposed a novel motion force control strategy in the framework of projection recurrent neural networks. Dang et al. [4] proposed a novel coordinated adaptive cruise control system to address the problem caused by a conventional ACC system. Zhao et al. [5] proposed an estimate of the benefit of the AEB systems for further enhancing the development. Ren et al. [6] proposed an integrated path tracking control framework for autonomous electric vehicles. Zhou et al. [7] proposed a control strategy for vehicle stability control. Li et al. [8] designed an obstacle avoidance controller for autonomous vehicle navigation. Wang et al. [9] presented an automatic lane change motion planning system targeting on discretional lane change motion planning scenario. Zhang et al. [10] proposed a novel motion planning to enhance the performance of the active collision avoidance systems of autonomous vehicles. Hang et al. [11] designed a linear parameter-varying H∞ controller designing for autonomous ground vehicles. Wang et al. [12] established an autonomous lane change motion planning decision-making model. Huang et al. [13] presented a novel local motion planning framework for vehicles following a trajectory. Wang et al. [14] presented a new path following the control approach to realize coordinated lateral and longitudinal control. Zhang et al. [15] developed a novel autonomous tracking control of intelligent electric vehicles to implement accurate path tracking. Peng et al. [16] proposed a new safe lane change motion planning trajectory model and collision avoidance control method for automatic driving vehicles. Funke et al. [17] presented a new control structure that integrated path tracking and vehicle stabilization. Wei et al. [18] developed a control framework to fulfill the automated vehicle. Xing et al. [19] provided an overview of the ego-vehicle driver intention inference focusing on the lane change motion planning intention on highways. To account for nonideal communication such as time-varying delays, Liu et al. [20] proposed an integrated vehicle-following control scheme for FWID EVs. Zhang et al. [21] provide a complete and systematic survey on chassis coordinated control methods for full X-by-wire vehicles. To mitigate the adverse influence of front-wheel steering angle sensor faults, Zhang et al. [22] proposed a new control method for SBW. Focused on the time-optimal multivehicle trajectory planning problem, Li et al. [23] provided an adaptive-scaling constrained optimization method. Focused on the multivehicle motion planning problem, Li et al. [24] provided a decentralized motion planning method for cooperative lane change motion planning of connected and automated vehicles. To facilitate the numerical solving process of the centralized optimal control problem, Li et al. [25] proposed a progressively constrained dynamic optimization method.

This paper proposes a hybrid optimization scheme based on the dynamic adaptive salp algorithm and Gaussian pseudospectral method (GPM) aiming to solve the problem of optimal lane change motion planning steering. The remainder of the paper is organized as follows. Section 2 presents a mathematical model of the lane change motion planning problem of the vehicle. Section 3 and Section 4 provide the hybrid algorithm, and Section 5 presents numerical simulations and virtual experimental verification. Finally, Section 6 concludes the paper and provides future research directions.

2. Mathematical Model of Vehicle Lane Change Motion Planning Problem

2.1. Mathematical Model of Vehicle Lane Change Motion Planning Problem. The vehicle lane change motion planning problem can be described as a 4-DOF vehicle model which has greater practical significance for theoretical analysis shown in Figure 1 [26].

In state-space form it is given by:

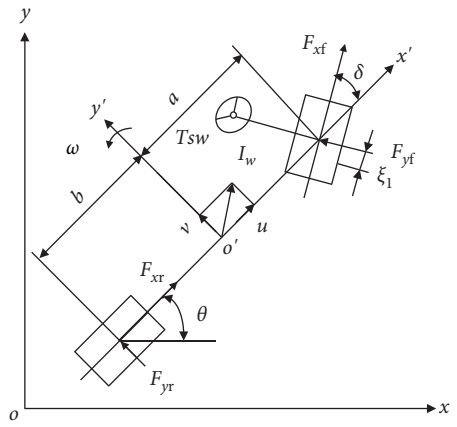

Figure 1: 4-DOF vehicle model.

$$\begin{cases} \dot{u} = v\omega + \dfrac{F_{xf}\cos\delta - F_{yf}\sin\delta + F_{xr} - F_f - F_w}{m} \\ \dot{v} = -u\omega + \dfrac{F_{yf}\cos\delta + F_{yr} + F_{xf}\sin\delta}{m} \\ \dot{\omega} = \dfrac{aF_{yf}\cos\delta - bF_{yr} + aF_{xf}\sin\delta}{I_z} \\ \dot{\delta} = p \\ \dot{p} = -\dfrac{k_1\xi_1}{I_w u}v - \dfrac{k_1\xi_1 a}{I_w u}\omega + \dfrac{(k_1\xi_1 - k_w)}{I_w}\delta - \dfrac{c_w}{I_w}p + \dfrac{T_{sw}i}{I_w} \end{cases}. \tag{1}$$

The parameters and the corresponding definitions can be found in Table 1.

The lateral forces of the front and rear tires are as follows:

$$\begin{cases} F_{yf} = k_1\left(\dfrac{v + a\omega}{u} - \delta\right)\sqrt{1 - \left(\dfrac{F_{xf}}{\mu F_{zf}}\right)^2 + \left(\dfrac{F_{xf}}{k_1}\right)^2} \\ F_{yr} = k_2\left(\dfrac{v - b\omega}{u}\right)\sqrt{1 - \left(\dfrac{F_{xr}}{\mu F_{zr}}\right)^2 + \left(\dfrac{F_{xr}}{k_2}\right)^2} \end{cases}, \tag{2}$$

where k_1 and k_2 are the synthesized stiffness of the front and rear tires, μ is the coefficient of friction, F_{yf} and F_{yr} are the lateral forces of front and rear tires.

The vertical forces of the front and rear wheels are as follows:

$$\begin{cases} F_{zf} = \dfrac{mgb - (F_{xf} + F_{xr})h_g}{a + b} \\ F_{zr} = \dfrac{mga + (F_{xf} + F_{xr})h_g}{a + b} \end{cases}. \tag{3}$$

Table 1: Parameter and definition.

Parameter	Definition
v	Lateral and longitudinal speed
u	Lateral and longitudinal speed
ω	Yaw rate of the vehicle
m	Vehicle mass
I_z	Moment of inertia around the z axis
k_w	Synthesized cornering stiffness
I_w	Moment of inertia of the steering system
a	Distances of front axle from the center of gravity
b	Distances of rear axle from the center of gravity
F_w	Air resistance
i	Transmission ratio of the steering system
c_w	Drag coefficient
ξ_1	Front wheel aligning arm of force
δ	Front steering angle
p	Steering rate
T_{sw}	Steering torque

where h_g is the height of the center gravity, F_{zf} and F_{zr} are the vertical forces of the front and rear wheels, F_{xf} and F_{xr} are the traction or brake forces of front and rear wheels.

To calculate the vehicle positions in the Earth coordinate defined by x and y, the vehicle velocity in the body coordinate is projected in the Earth coordinate as:

$$\begin{cases} \dot{x} = u\cos\theta - v\sin\theta \\ \dot{y} = v\cos\theta + u\sin\theta \end{cases}, \tag{4}$$

where θ is the heading angle of the vehicle.

According to Eq. (1) and Eq. (4), the state equation can be described as:

$$\dot{x} = f[x(t), z(t)], \tag{5}$$

where $x(t)$ and $z(t)$ are the state and the input which are denoted respectively as $x(t) = [u(t), v(t), \omega(t), \delta(t), p(t), x(t), y(t), \theta(t)]^T$, $z(t) = [T_{sw}(t)]^T$.

2.2. Longitudinal Safety Distance Model. The vehicle steering and lane change motion planning maneuver model is shown in Figure 2. When a driving vehicle encounters an obstacle in front of the same lane, the driver adopts the method of steering and change lanes to avoid the obstacle. And the lane change motion planning process is shown in Figure 3.

The safety distance model based on braking process is as follows:

$$S_0 = S_1 + S_2 + S_3, \tag{6}$$

where S_0 is the minimum safety distance between the leading vehicle and the following vehicle; $S_1 = u(t_1 + t_2)$, where S_1 is the distance traveled by the following vehicle; $S_2 = ut_3 - 1/6a_0t_3^2$, where S_2 is the distance traveled by the following vehicle in t_3; $a_0 = \varphi g$; $S_3 = u^2/2a_0 - 1/2ut_3 + 1/8a_0t_3^2$, where S_3 is the distance traveled by the following vehicle in t_4 .

2.3. Optimal Control Object of Lane Change Motion Planning Problem. The minimum time problem of lane change motion planning can be regarded as the optimal control

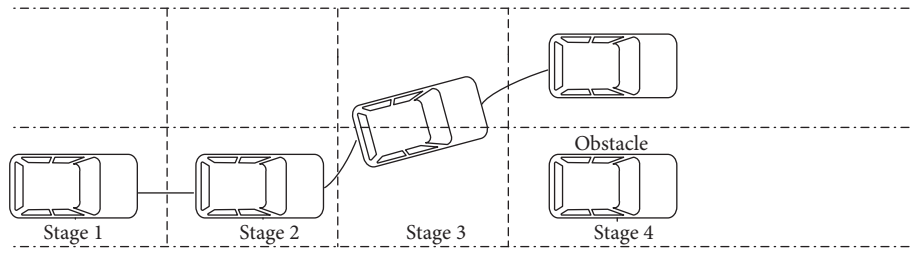

Figure 2: Model of vehicle lane change motion planning.

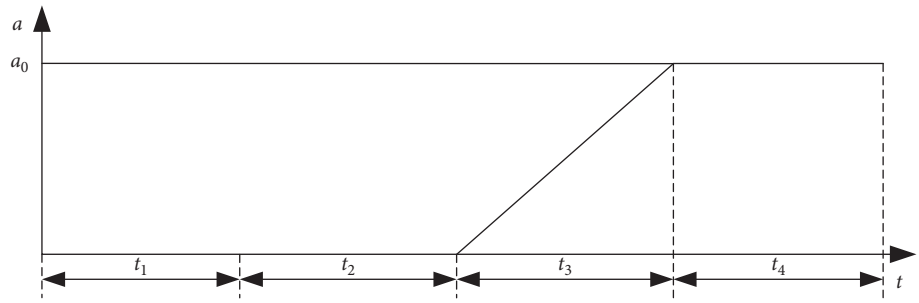

Figure 3: Lane change motion planning process.

problem in the control theory. Therefore, the minimum time performance indicator is as follows:

$$J = \int_{t_0}^{t_f} dt, \tag{7}$$

where $D_{ki}(\tau_k) = \dot{L}(\tau_k) = \{ (1+\tau_k)\dot{P}_N(\tau_k) + P_N(\tau_k)/(\tau_k - \tau_i)[(1+\tau_i)\dot{P}_N(\tau_i) + P_N(\tau_i)], i \neq k(1+\tau_i)\dot{P}_N(\tau_i) + 2\dot{P}_N(\tau_i)/2[(1+\tau_i)\dot{P}_N(\tau_i) + P_N(\tau_i)], i = k$ is the initial time, $D_{ki} \in R^{N\times(N+1)}$ is the final time.

2.4. Constrains. The initial and terminal states are described as:

$$x(t_0) = [u_0, 0, 0, 0, 0, 0, 0, 0]^T. \tag{8}$$

$$x(t_f) = [u_0, 0, 0, 0, 0, x_f, y_f, 0]^T. \tag{9}$$

To accomplish the lane change motion planning maneuver successfully, the constraints set on the longitudinal and lateral distance as well as the lateral acceleration are $0 \le x \le x_b$, $B_0 \le y \le B_1$, $|a_y| \le 3m/s^2$. Where x_b is the longitudinal distance between vehicle and obstacle; B_0 and B_1 are the minimum lateral displacement required for completing the lane change motion planning process and the left boundary of adjacent lane, respectively.

When the braking maneuver is applied to decelerate the vehicle, the constraints on F_{xf}, F_{xr} can be rewritten in the following manner:

$$\left.\begin{aligned} F_{xf} &\ge -\frac{\mu m g(b + \mu h_g)}{a+b} \\ F_{xr} &= \frac{a - \mu h_g}{b + \mu h_g} F_{xf} \end{aligned}\right\}. \tag{10}$$

The boundary constraint of the control variable is decided by the driver's physiological limit as:

$$z_{\min} \le z \le z_{\max}, \tag{11}$$

where $z_{\min}$ and $z_{\max}$ are the lower and upper limit values of the steering torque.

3. Salp Swarm Algorithm and GPM

3.1. Salp Swarm Algorithm. Inspired by the navigation and predation behavior of marine creature salps, Mirjalili proposed the salp swarm algorithm(SSA) and used it to solve the optimization problem. Specifically, the entire population of salps is divided into leaders and followers. The leader is responsible for leading the entire population, and the followers follow each other. In this way, the entire population gradually moves to the food position (i.e., the global optimal point). The position of the leader is updated by the following formula:

$$x_j^1 = \begin{cases} F_j + c_1(l)\left[\left(ub_j - lb_j\right)c_2 + lb_j\right]c_3 & \ge 0.5 \\ F_j - c_1(l)\left[\left(ub_j - lb_j\right)c_2 + lb_j\right]c_3 & < 0.5 \end{cases}, \tag{12}$$

where x_j^1 is the position of the j^{th} dimension of the leader; f_j is the position of the j^{th} dimension of the food; $c_1(l) = 2\exp[-(4l/L)^2]$ balances the process of exploration and utilization; l is the current number of iterations; L is the maximum number of iterations; c_2 and c_3 are random numbers uniformly distributed in interval $[0, 1]$; and ub_j and lb_j represent the upper and lower bounds of the j^{th} dimension respectively. It is worth noting that the global optimal solution is usually unknown, so the currently obtained optimal solution is taken as the global optimal solution. The position of the follower is updated by the following formula:

$$x_j^i = \frac{1}{2}\left(x_j^i + x_j^{i-1}\right), \tag{13}$$

where $i \geq 2$, x_j^i represents the position of the i^{th} follower in the j^{th} dimension. If the position of the individual exceeds the search space, it is corrected to return to the search space.

3.2. GPM. First, the basic principle of GPM is introduced briefly. The state and control variables in the kinematics equation are discreted on a series of Gauss points, which are taken as nodes to construct Lagrange interpolation polynomials to approximate the state and control variables. The derivative of the state variable with respect to time is approximated by taking the derivative of the global interpolation polynomial. In this way, the differential equation constraints are transformed into a set of algebraic constraints. The terminal state can be represented by the initial state and the Gaussian integral jointly. And the integral part of the objective function can also be represented by the Gaussian integral. Then, the optimal control problem can be transformed into an NLP problem with a series of algebraic constraints.

For the sake of convenience, the optimal lane change motion planning problem is transformed into a Bolza problem.

The Bolza cost function is as follows:

$$J = \psi\left(x(t_0), t_0, x\left(t_f\right), t_f\right) + \int_{t_0}^{t_f} g(x(t), z(t), t)dt. \tag{14a}$$

The dynamic constrain is given by:

$$\dot{x} = f(x(t), z(t), t) \quad t \in \left[t_0, t_f\right]. \tag{14b}$$

The boundary constrain is as follows:

$$\varphi\left(x(t_0), t_0, x\left(t_f\right), t_f\right) = 0. \tag{14c}$$

The inequality path constraint is shown as:

$$C[x(t), z(t), t] \leq 0 \quad t \in \left[t_0, t_f\right], \tag{14d}$$

where $x(t) \in R^n$ is the state, and $z(t) \in R^m$ is the input.

3.2.1. Time Domain Transformation. Since the orthogonal interval of the orthogonal polynomial involved is $\tau \in [-1, 1]$, it is necessary to convert the time interval $[t_0, t_f]$ to [–1, 1] when using GPM to solve the optimization problem.

The time variable t is transformed as follows:

$$\tau = \frac{2t}{\left(t_f - t_0\right)} - \frac{t_f + t_0}{\left(t_f - t_0\right)}. \tag{15}$$

3.2.2. Approximation of State and Control Variables. The collocation points $\tau_k (k = 1, 2, \cdots, N)$ of the GPM are the N LG points. That is the roots of the N^{th}-order Legendre polynomial. The distribution interval of collocation points is (–1, 1). So there are $N+1$ nodes when adding the boundary point $\tau_0 = -1$. Then, the state variable $x(\tau)$ can be approximated by a combination of $N+1$ Lagrange interpolation polynomials.

$$\begin{cases} x(\tau) \approx X(\tau) = \sum_{i=0}^{N} L_i(\tau) X(\tau_i), \\ \\ L_i(\tau) = \prod_{j=0, j\neq i}^{N} \dfrac{\tau - \tau_j}{\tau_i - \tau_j}. \end{cases} \tag{16}$$

Similarly, the control variable $z(\tau)$ can be approximated by a combination of N Lagrange interpolation polynomials.

$$\begin{cases} z(\tau) \approx Z(\tau) = \sum_{i=1}^{N} L_i^*(\tau) Z(\tau_i), \\ \\ L_i^*(\tau) = \prod_{j=1, j\neq i}^{N} \dfrac{\tau - \tau_j}{\tau_i - \tau_j}. \end{cases} \tag{17}$$

3.2.3. Differential Equation Constraints. Equation (24) can be obtained by differentiating Eq. (22):

$$\begin{aligned} \dot{x}(\tau_k) \approx \dot{X}(\tau_k) &= \sum_{i=0}^{N} \dot{L}_i(\tau_k) X(\tau_i) \\ &= \sum_{i=0}^{N} D_{ki} X(\tau_i), \end{aligned} \tag{18}$$

where $D_{ki} \in R^{N\times(N+1)}$ is an $N\times(N+1)$ state differential matrix:

$$\begin{aligned} D_{ki}(\tau_k) &= \dot{L}(\tau_k) \\ &= \begin{cases} \dfrac{(1+\tau_k)\dot{P}_N(\tau_k) + P_N(\tau_k)}{(\tau_k - \tau_i)\left[(1+\tau_i)\dot{P}_N(\tau_i) + P_N(\tau_i)\right]}, & i \neq k, \\ \\ \dfrac{(1+\tau_i)\ddot{P}_N(\tau_i) + 2\dot{P}_N(\tau_i)}{2\left[(1+\tau_i)\dot{P}_N(\tau_i) + P_N(\tau_i)\right]}, & i = k, \end{cases} \end{aligned} \tag{19}$$

where $P_N(\tau_k)$ is N^{th}-order Legendre polynomial.

Then, the dynamic differential equation constraints are transformed into algebraic constraints:

$$\sum_{i=0}^{N} D_{ki} X(\tau_i) - t_f - t_0/2 f\left(X(\tau_k), Z(\tau_k), \tau_k; t_0, t_f\right) = 0. \tag{20}$$

3.2.4. Terminal State Constraints. Since the approximation of the state variable in Eq. (15) ignores the terminal time τ_f, the terminal state constraints need to be supplemented:

$$x\left(\tau_f\right) = x(\tau_0) + \int_{-1}^{1} f(x(\tau), Z(\tau), \tau)d\tau. \tag{21}$$

The following equation can be obtained by discreting the terminal constraints and approximating them with Gauss integration.

$$X\left(\tau_f\right) = X\left(\tau_0\right) + \frac{t_f - t_0}{2} \sum_{k=1}^{N} \omega_k f\left(X\left(\tau_k\right), Z\left(\tau_k\right), \tau_k; t_0, t_f\right). \tag{22}$$

3.2.5. Approximation of Objective Function. Approximating the integral term in the objective Equation (14a) with Gauss integral, the following equation can be obtained:

$$J = \Phi\left(X_0, t_0, X_f, t_f\right) + \frac{t_f - t_0}{2} \sum_{k=1}^{N} \omega_k g\left(X_k, Z_k, \tau_k; t_0, t_f\right). \tag{23}$$

The boundary condition constraints equation (14c) and inequality constraints (14d) are discretized as:

$$\varphi\left(X\left(\tau_0\right), t_0, X\left(\tau_f\right), t_f\right) = 0, \tag{24}$$

$$C\left[X\left(\tau_k\right), Z\left(\tau_k\right), \tau_k; t_0, t_f\right] \le 0. \tag{25}$$

After the above transformation, the original optimal control problem is transformed into an NLP problem.

4. Optimal Lane Change Motion Planning Steering based on Dynamic Adaptive Salp Swarm Algorithm(DASSA) and GPM

4.1. Dynamic Adaptive Salp Swarm Algorithm. In essence, intelligent optimization algorithms face the problem of falling into local optimum. Therefore, improvement strategies are developed around the exploration and utilization process of balancing algorithm optimization avoiding falling into local optima.

It can be seen from Eq. (12) that the coefficient $c_1(l)$ is the main parameter to be explored and utilized in the balance optimization process. As the number of iterations increases, $c_1(l)$ keeps decreasing. To make the population evolve more reasonably, based on the traditional SSA algorithm, this section draws on the "feedback" idea in the classic control theory, introducing the population improvement rate as the feedback variable to adaptively update the coefficient $c_1(l)$, and proposing a novel DASSA optimization algorithm.

The improvement rate of the population is defined as $R = M_s/M$, where M_s is the number of individuals in the current population that are closer to the global optimal solution than the previous generation. M is the population size. According to the 1/5 principle, the algorithm parameters should be dynamically and adaptively changed to make the population improvement rate be 20%. Therefore, when $R0.2$, it indicates that the exploration ability is strong, but the utilization ability is weak. And $c_1(l)$ should be reduced to improve search accuracy. When $R > 0.2$, the population is mainly performing local optimization. And $c_1(l)$ should be increased at this time to improve the global search capability. When $R = 0.2$, exploration and utilization have reached a reasonable balance. So, there is no need to adjust $c_1(l)$ dynamically.

The above dynamic adaptive rules can be expressed as:

$$c_1(l) = \begin{cases} c_1(l-1) \cdot \zeta, R0.2 \\ c_1(l-1), 0.2 \le R \le 0.3 \\ \dfrac{c_1(l-1)}{\zeta}, R0.3 \end{cases}. \tag{26}$$

where $c_1(l-1)$ is the adjustment factor of the last iteration; $0\zeta1$ is the learning factor.

It should be noted that in (26), there is no need to adjust the range of $c_1(l)$ from $R = 0.2$ expand to $0.2 \le R \le 0.3$. This is because that the probability of occurrence of $R = 0.2$ is very low, resulting in frequent changes of $c_1(l)$, which is not conducive to the stability of parameter self-adjustment.

4.2. Treatment of Constraint Conditions Based on Penalty Function Method. The SSA optimization algorithm is originally proposed to solve the static optimization problem without constraints. And the lane change motion planning optimization problem contains a variety of constraints, which cannot be solved directly by the SSA algorithm. So, the constraints need to be processed. Generally speaking, the penalty function method is the most common constraint processing method, which has the advantages of simple principle and easy implementation. Therefore, in the optimization process using the DASSA algorithm, the fitness function can be defined as the objective function combined with the penalty function, which is expressed as follows:

$$F(x) = J + P(x), \tag{27}$$

where J is the objective function; $P(x)$ is the penalty function, which can be expressed as:

$$P(x) = \sum_{k=1}^{N} \left[P_h(x) + P_d(x) + P_1(x) + P_b(x) + P_f(x)\right], \tag{28}$$

where N is the number of discrete points in the optimization process; $P_b(x)$ and $P_f(x)$ are the penalty functions of exceeding the boundary and the terminal state constraints, respectively, which are expressed as:

$$P_b(x) = \sum_{i=1}^{2} \left(|\overline{\overline{\eta}}(b(i) - b(i))/b(i)|^{\lambda} + |\overline{\eta}(b(i) - \overline{b}(i))/\overline{b}(i)|^{\lambda}\right), \tag{29}$$

$$P_f(x) = \sum_{i=1}^{6} \left|\eta\left(x(i) - x_f(i)\right)/x_f(i)\right|, \tag{30}$$

where λ and η are both penalty coefficients; $\overline{\overline{\eta}}$ and $\overline{\eta}$ are defined as:

$$\overline{\overline{\eta}} = \begin{cases} \eta x, & x \le 0 \\ 0, & x0 \end{cases}. \tag{31}$$

$$\overline{\eta} = \begin{cases} \eta x, & x \ge 0 \\ 0, & x0 \end{cases}. \tag{32}$$

4.3. Optimization Program of DASSA-GPM Algorithm. Aiming at the optimization problem of lane change motion planning steering, the DASSA-GPM hybrid optimization algorithm is used to solve the optimal control variables. Specifically, the entire optimization process is divided into two stages. In the first stage, the DASSA optimization algorithm is used to perform a global optimization of the control variables, which can make full use of the global search ability of the intelligent optimization algorithm and avoid falling into the local optimum. When the change value of the fitness function reaches the preset stopping standard, the optimization process of the DASSA algorithm is stopped. And the approximate global optimal solution obtained is used as the initial guess value of the GPM optimization. In the second stage, GPM is used to optimize the control variables globally, so that it is convenient to take advantage of the advantages of fast convergence speed and high accuracy of GPM.

The detailed steps of the DASSA-GPM optimization algorithm are as follows:

Step 1:

(1) Formulating the optimization problem of lane change motion planning steering.

(2) Setting the parameters of the DASSA-GPM optimization algorithm.
It is set that the maximum number of iterations is L, the population size is M, the number of discrete LG points is N, the stop standard of the DASSA algorithm is e_{DASSA} , and the stop standard of the GPM algorithm is e_{GPM}.

(3) Discreting the time interval $[t_0, t_f]$ with NLG points equidistantly.
The control variable $u = [\alpha, \delta]^T$ is set as the variable to be optimized. The position of each population individual represents the optimized value of a group of control variables. The complete information of the population can be expressed as a matrix:

$$X = [X_1, \cdots, X_n, \cdots, X_N], \tag{33}$$

where the optimized matrix of the discrete point n is:

$$X_N = \begin{bmatrix} \alpha_{n1} & \sigma_{n1} \\ \vdots & \vdots \\ \alpha_{nm} & \sigma_{nm} \\ \vdots & \vdots \\ \alpha_{nM} & \sigma_{nM} \end{bmatrix}, \tag{34}$$

where α_{nm} represents the attack angle of the m^{th} population at the n^{th} discrete point; σ_{nm} represents the inclination angle of the m^{th} population at the n^{th} discrete point.

(4) Randomly initializing the positions of M population individuals within the constraints.

(5) Based on the discrete position information of the population individuals, the system state and the differential of the state are obtained through interpolation integration. And then the fitness function value of each population individual is calculated.

(6) Updating the positions of all population individuals, and updating the global and local optimal values.

(7) The DASSA algorithm optimization process is stopped if the maximum number of iterations or the stop standard of the DASSA algorithm e_{DASSA} is reached, saving the currently obtained optimal control variables and related state variables, then going to 8); otherwise, returning to 5).

Step 2:

(8) The control variables obtained by optimization of the DASSA algorithm at discrete points is used as the initial guess values of GPM. The relevant parameters in the GPM optimization process, such as variable range, boundary range, and discrete LG points, remain unchanged.

(9) After converting the lane change motion planning steering optimization problem into an NLP problem through GPM, the NLP solver is used to solve the optimization problem. The GPM algorithm optimization process is stopped if the stop standard e_{GPM} of the GPM is reached.

(10) Using the obtained optimal control variables u^* to integrate Eq. (1) to obtain the system state variables, from which the optimal control and state variables in the optimization process can be obtained.

(11) If the calculation time and cost function value meet the conditions, the simulation process ends; otherwise, adjusting the number of discrete LG points N and returning to 3.

It should be pointed out that the optimization process is completed off-line. The DASSA-GPM algorithm has more steps than the GPM algorithm, but it does not affect the real-time performance of the optimization process.

5. Numerical Simulations and Experimental Verification

5.1. Numerical Simulations. To verify the effectiveness of the method proposed in this paper, the simulations using MATLAB is established. In the simulation, the parameters of the vehicle are according to Reference 26.

5.1.1. Lane Change Motion Planning Condition. Figures 4(a)–4(e) show the results of the steering wheel angle rate, the steering wheel angle, the lateral distance, and the

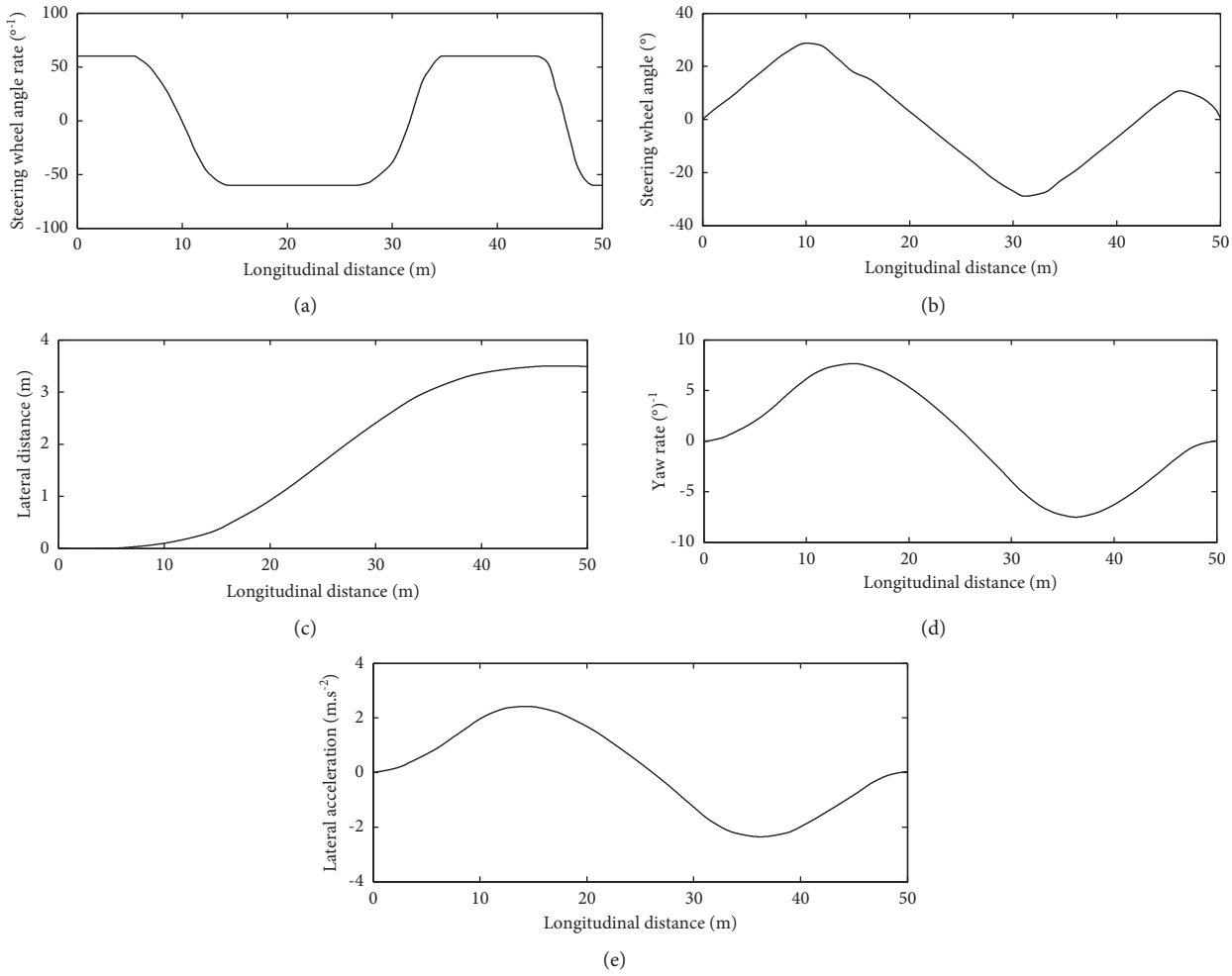

Figure 4: Simulation results of the estimated values between the state variables under the lane change motion planning condition. (a) Steering wheel angle rate, (b) Steering wheel angle, (c) Lateral distance, (d) Yaw rate, and (e) Lateral acceleration.

yaw rate as well as the lateral acceleration under the lane change motion planning condition.

It can be seen from Figure 4(a) that the steering wheel angle rate produces amplitudes at longitudinal distances of 6 m, 14 m, 28 m, 34 m, 44 m, and 48 m, indicating that the busyness degree of the driver is greater between the first and second turns when taking the lane change motion planning maneuver. This is because the driver needs quicker actions to maneuver the vehicle from finding the vehicle ahead to change lanes to the adjacent lane in the shortest time.

Figure 4(b) proves that the steering angle of the front wheel can be controlled under constrained conditions. The result indicates that under the condition of a higher friction coefficient, the performance of lane change motion planning avoidance by steering depends on the upper limit of the steering rate of the front wheel.

Figure 4(c) shows that the vehicle completes the lane change motion planning process after 50 m under the constraint conditions to avoid the obstacle ahead and achieve a good control effect, ensuring the safety of the vehicle.

Figure 4(d) shows that the yaw rate of the vehicle peaks when it starts to change lane and change to the adjacent lane for body alignment when the vehicle is prone to sideslip or tail drift. After about 50 m, the vehicle gradually entered a stable state.

Figure 4(e) indicates that by constraining the vehicle dynamics, the lateral acceleration of the vehicle does not have an obvious overshoot during the lane change motion planning process, which meets the requirements of vehicle stability.

5.1.2. Double Lane Change Condition. In real traffic conditions, the double lane change road which demonstrates the overtaking performance of the vehicle is the basic working conditions.

Figure 5 shows the results of the yaw rate and the lateral acceleration as well as the steering wheel angle under the double lane change road condition with the initial speed of 108 km/h.

From Figure 5(a), it can be seen that the yaw rate of the vehicle peaks when passing through the first and second

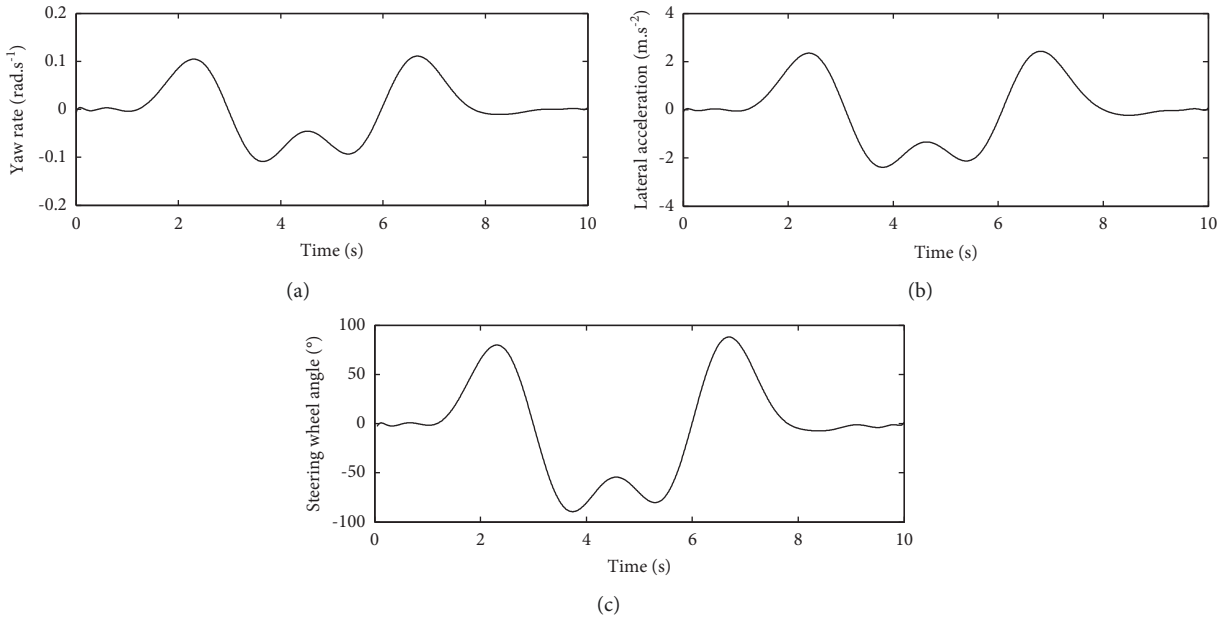

Figure 5: Simulation results of the estimated values between the state variables under the double lane change condition. (a) Yaw rate, (b) Lateral acceleration, and (c) Steering wheel angle.

corners, and the driver should control the steering wheel and vehicle speed to prevent sideslip or drift. After the third corner, the vehicle gradually reaches a steady state.

And also, it can be seen from Figure 5(b) that the lateral acceleration has bigger response values at 2.5 s, 3.8 s, 5.5 s, and 6.8 s, which indicates that the vehicle will yield bigger lateral acceleration when it enters and moves away from the double lane change road.

From Figure 5(c), it is also shown that the steering wheel angle is larger at 2.5 s, 3.8 s, 5.5 s, and 6.8 s, which indicate that the driver is busy at the time. So the driver of the vehicle has a slightly heavier burden.

5.2. Accuracy and Efficiency Verification. To verify the superiority of the method proposed in this paper, comparison results between the DASSA-GPM and the traditional GPM method which are shown in Figure 6 are proposed.

Figures 6(a) and 6(b) show the simulation results of the steering wheel angle rate and the steering wheel angle obtained by DASSA-GPM and GPM methods for solving the lane change motion planning problem in the same conditions. It can be found that the trend of the curves both of the steering wheel angle rate and the steering wheel angle obtained by DASSA-GPM and GPM methods is consistent. However, it can be seen from Figure 6(c) that the absolute error of steering wheel angle calculated by the DASSA-GPM is smaller than that of the GPM method indicating the superiority of the method proposed in this paper.

A comparison is implemented to verify the computational accuracy of the presented scheme under the same simulation condition. The comparison result of the calculation accuracy is shown in Table 2. From Table 2, it can be seen that the calculation efficiency of DASSA-GPM is higher than GPM under the same calculation accuracy. However, with the improvement of calculation accuracy, both the DASSA-GPM and GPM method have a higher calculation burden. So, the calculation accuracy of this paper is set to be 10^{-3}.

5.3. Experimental Verification. A virtual test adopting the Carsim software is conducted to verify the feasibility of the simulated results.

Carsim is a software product of a mechanical simulation company that simulates vehicle behavior. It can perform three-dimensional dynamic vehicle response, advanced controllers, interaction between driver control and three-dimensional road. It can be easily used by most engineers and technicians. Each package contains VS browser (GUI and database management), VS visualizer (animation and plotting), online help and VS solver for detailed mathematical models. And the mathematical models can be run stand-alone or using third-party simulation software such as Simulink, LabVIEW. In essence, the software first builds a vehicle model and then sets parameters according to its simulation content. The simulation results are displayed through 3D animation or tabular data after processor operation. The test speed is many times faster than the actual test speed by using the software for simulation. The software can be used to simulate the feedback of the vehicle under various inputs of driver and ground conditions and can be used to help improve the handling, braking, ride comfort, power, and economy of the vehicle. At present, it is adopted by many large automobile manufacturers. It has become the standard software for vehicle dynamics analysis. The simulation results have high reliability. Carsim main interface is divided into three parts: Vehicle & Procedure module, RunControl module, and Results (Post Processing) module. The first part is the vehicle model and operating conditions.

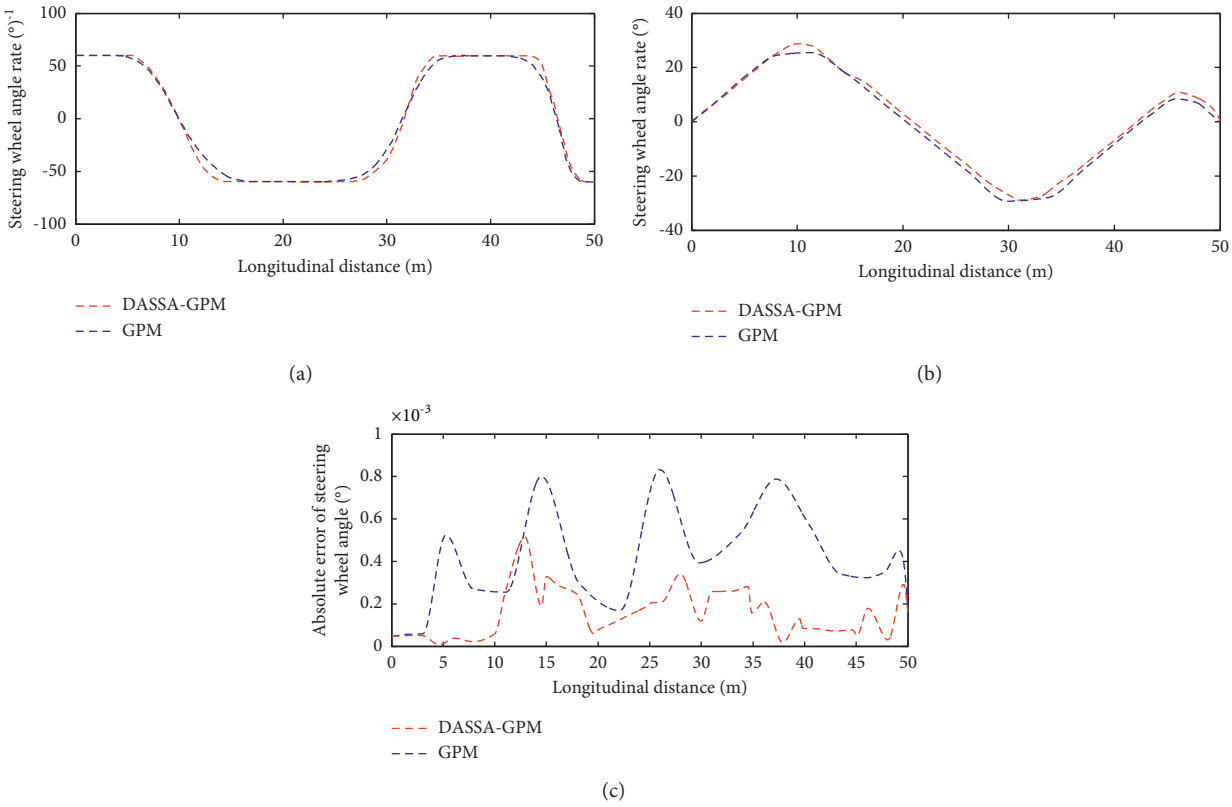

Figure 6: Comparison results between DASSA-GPM and GPM. (a) Steering wheel angle rate, (b) Steering wheel angle, and (c) Absolute error of steering wheel angle.

Table 2: Evaluation of the calculation efficiency.

Computation accuracy	Calculation time(s)	
	DASSA-GPM	GPM
10^{-2}	1.31	1.35
10^{-3}	3.86	4.81
10^{-4}	9.73	10.89

There are complete vehicle model, driver input model, and external environment model. The internal data is general. The experimenter can modify the parameters of the built-in model to simulate the test vehicle, which reduces the difficulty of modeling. For different test vehicles, the experimental simulation can be carried out by modifying the relevant parameters. And considerable experimental accuracy can be obtained. The second part is the mathematical solver module. Carsim has a built-in mathematical solver. At the same time, it can also establish C language joint simulation model through DLL file or Simulink joint simulation through Carsim s-function, which has strong expansibility. The third part is the operation results and postprocessing module. The simulation results can be output by a curve or three-dimensional animation. At the same time, multiple models can be run at the same time. Compare the output results to visually display the impact of different parameters on the target parameters.

Since the Carsim model runs three to six times faster than real time on the computer, it is possible to simulate the response of the vehicle to the driver, road surface, and aerodynamic inputs, thereby predicting the handling stability, braking, ride comfort, and fuel economy of the vehicle. At present, due to its development cost and the accuracy of the model, more and more modern automobile manufacturers and research institutes use it to develop control strategies.

The main features of the Carsim software are as follows:

5.3.1. The Model Is Accurate. The vehicle model of Carsim is based on the dynamic characteristics of the entire vehicle. And with the in-depth study of the dynamics, the software will continue to update the model. And most of the simulation reference data are compared with the real test. So the simulation results of Carsim have a certain reference value.

5.3.2. Expansion Is Diversified. Since Carsim is more than just research on vehicles, it also includes the common analysis and modeling of the three traffic elements: people, vehicles, and road. So its parameter input is complex and diverse. To facilitate the needs of customers, Carsim has cooperated with Mathworks and National Instruments (NI) to combine MATLAB/Simulink, Lab VIEW, and other software commonly used in the development of control strategies, expanding many common interfaces and greatly shortening research. It reduces the time for personnel modeling and reduces the difficulty for researchers to use the

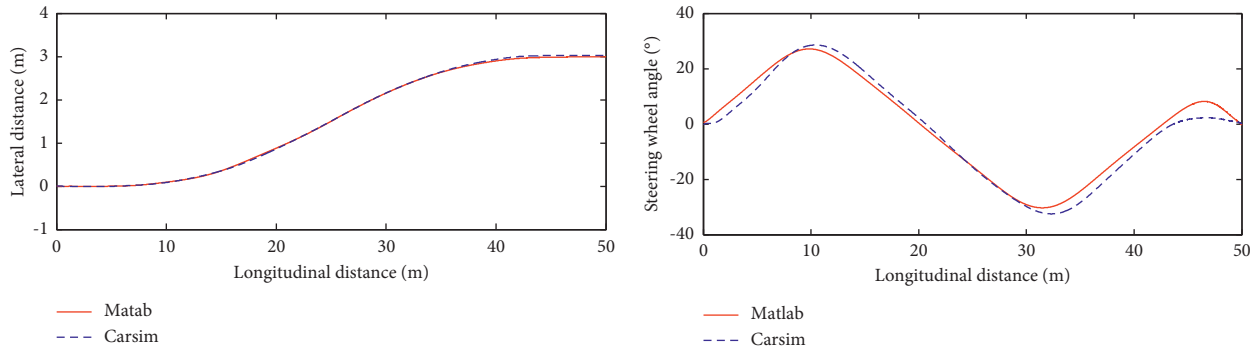

Figure 7: Experimental results of the lateral distance and the steering wheel angle. (a) Lateral distance and (b) Steering wheel angle.

software. And researchers can directly combine their algorithms with the Carsim vehicle model for simulation verification.

5.3.3. There Are Many Development Libraries. Carsim has a development kit research that keeps pace with the times. It will improve its software with the growth of the number of customers and the development of automotive industry trends, and develop a development library suitable for contemporary application needs, including tires, brakes, driver, powertrain, and a series of traditional auto parts as well as sensors, pedestrians, and obstacle models required for intelligent driving.

5.3.4. The Simulation Results Are Visible. For Carsim, a large number of instance data sets and animated graphics make it more authoritative and vivid. Carsim has developed its 3D outline drawings for 15 different models, which can meet all daily model research and can also modify the models according to their own needs. At the same time, animation verification can be performed after the simulation is completed, which makes the dynamic simulation more visual. For the simulation basis of the results, it also provides the function of automatic generation of icons, which is fully prepared for the customer's further research.

5.3.5. The Software Is Easy to Use. With the continuous upgrading of the software, Carsim not only expands diversified algorithm software but also uses multiple languages to facilitate customers to build their models. In Carsim, customers can use C language to modify the algorithm or model parameters according to their own needs and also can use simple mouse clicks to select and modify the drop-down menu.

From Figure 7 it can be seen that there are errors between the simulation and the virtual test values for both the lateral distance and the steering wheel angle. This is because the established vehicle model does not fully reflect the true performance of the vehicle. However, from Figure 7, it can also be seen that the simulation curves of the lateral distance and the steering wheel angle obtained by the DASSA-GPM algorithm is consistent with that of the virtual test curves obtained by the Carsim. So the results can verify the correctness of the proposed method.

6. Conclusions

In this paper, based on a 4-DOF nonlinear vehicle dynamics model, a novel DASSA-GPM algorithm is used to solve the problem of optimal lane change motion planning. The calculation results show that the DASSA-GPM method proposed in this paper has potential advantages in solving the optimal steering input problem of complex and multi-constrained vehicle running trajectories and can better control the vehicle along the given desired lane change motion planning at high speed. It can successfully solve the problem of vehicle lane change motion planning maneuvering dynamics. The simulation values obtained by the DASSA-GPM algorithm are in good agreement with the virtual test values indicating the effectiveness of the method. By accuracy and efficiency verification compared with traditional method, the DASSA-GPM method proposed in this paper is verified to have higher precision and efficiency in solving nonsmooth problems.

In the near future, subsequent research will be devoted to the algorithm of a more accurate safe distance model and considering the change of vehicle speed under actual traffic conditions, so as to provide theoretical guidance for the research on improving the vehicle emergency collision avoidance control system.

Data Availability

The related data used to support the findings of this study are available from the corresponding author upon request.

Conflicts of Interest

The authors declare that they have no conflicts of interest.

Acknowledgments

This paper was supported by the Science and Technology Program Foundation of Weifang under Grant 2015GX007. The first author gratefully acknowledges the support agency.

References

[1] S. Cheng, L. Li, M.-M. Mei, Y.-L. Nie, and L. Zhao, "Multiple-objective adaptive cruise control system integrated with DYC," *IEEE Transactions on Vehicular Technology*, vol. 68, no. 5, pp. 4550–4559, 2019.

[2] P. Wang, S. Gao, L. Li, B. Sun, and S. Cheng, "Obstacle avoidance path planning design for autonomous driving vehicles based on an improved artificial potential field algorithm," *Energies*, vol. 12, no. 12, pp. 2342–2414, 2019.

[3] X. Li, Z. Xu, S. Li, Z. Su, and X. Zhou, "Simultaneous obstacle avoidance and target tracking of multiple wheeled mobile robots with certified safety," *IEEE Transactions on Cybernetics*, vol. 3, pp. 1–15, 2021.

[4] R. Dang, J. Wang, S. E. Li, and K. Li, "Coordinated adaptive cruise control system with lane-change assistance," *IEEE Transactions on Intelligent Transportation Systems*, vol. 16, no. 5, pp. 2373–2383, 2015.

[5] Y. Zhao, D. Ito, and K. Mizuno, "AEB effectiveness evaluation based on car-to-cyclist accident reconstructions using video of drive recorder," *Traffic Injury Prevention*, vol. 20, no. 1, pp. 100–106, 2019.

[6] Y. Ren, L. Zheng, and A. Khajepour, "Integrated model predictive and torque vectoring control for path tracking of 4-wheel-driven autonomous vehicles," *IET Intelligent Transport Systems*, vol. 13, no. 1, pp. 98–107, 2019.

[7] Y. Z. Zhou, R. C. Wang, R. K. Ding, D. Shi, and Q. Ye, "Investigation on hierarchical control for driving stability and safety of intelligent HEV during car-following and lane-change process," *Science China Technological Sciences*, vol. 65, pp. 1–24, 2021.

[8] S. Li, Z. Li, Z. Yu, B. Zhang, and N. Zhang, "Dynamic trajectory planning and tracking for autonomous vehicle with obstacle avoidance based on model predictive control," *IEEE Access*, vol. 7, Article ID 132074, 2019.

[9] J. Wang, H. Zheng, and C. Zong, "Longitudinal and lateral dynamics control of automatic lane change system," *Transactions of the Institute of Measurement and Control*, vol. 41, no. 15, pp. 4322–4338, 2019.

[10] Z. Zhang, L. Zheng, Y. Li, P. Zeng, and Y. Liang, "Structured road-oriented motion planning and tracking framework for active collision avoidance of autonomous vehicles," *Science China Technological Sciences*, vol. 64, no. 11, pp. 2427–2440, 2021.

[11] P. Hang, X. Chen, and F. Luo, "LPV/H∞ controller design for path tracking of autonomous ground vehicles through four-wheel steering and direct yaw-moment control," *International Journal of Automotive Technology*, vol. 20, no. 4, pp. 679–691, 2019.

[12] Y. Liu, X. Wang, L. Li, S. Cheng, and Z. Chen, "A novel lane change decision-making model of autonomous vehicle based on support vector machine," *IEEE Access*, vol. 7, Article ID 26543, 2019.

[13] Y. Huang, H. Wang, A. Khajepour, H. Ding, K. Yuan, and Y. Qin, "A novel local motion planning framework for autonomous vehicles based on resistance network and model predictive control," *IEEE Transactions on Vehicular Technology*, vol. 69, no. 1, pp. 55–66, 2020.

[14] Y. Wang, H. Ding, J. Yuan, and H. Chen, "Output-feedback triple-step coordinated control for path following of autonomous ground vehicles," *Mechanical Systems and Signal Processing*, vol. 116, pp. 146–159, 2019.

[15] X. Zhang and X. Zhu, "Autonomous path tracking control of intelligent electric vehicles based on lane detection and optimal preview method," *Expert Systems with Applications*, vol. 121, pp. 38–48, 2019.

[16] T. Peng, L. Su, R. Zhang et al., "A new safe lane-change trajectory model and collision avoidance control method for automatic driving vehicles," *Expert Systems with Applications*, vol. 141, Article ID 112953, 2020.

[17] J. Funke, M. Brown, S. M. Erlien, and J. C. Gerdes, "Collision avoidance and stabilization for autonomous vehicles in emergency scenarios," *IEEE Transactions on Control Systems Technology*, vol. 25, no. 4, pp. 1204–1216, 2017.

[18] S. Wei, Y. Zou, X. Zhang, T. Zhang, and X. Li, "An integrated longitudinal and lateral vehicle following control system with radar and vehicle-to-vehicle communication," *IEEE Transactions on Vehicular Technology*, vol. 68, no. 2, pp. 1116–1127, 2019.

[19] Y. Xing, C. Lv, H. Wang et al., "Driver lane change intention inference for intelligent vehicles: framework, survey, and challenges," *IEEE Transactions on Vehicular Technology*, vol. 68, no. 5, pp. 4377–4390, 2019.

[20] J. Liu, Z. Wang, and L. Zhang, "Integrated vehicle-following control for four-wheel-independent-drive electric vehicles against non-ideal V2X communication," *IEEE Transactions on Vehicular Technology*, vol. 71, no. 4, pp. 3648–3659, 2022.

[21] L. Zhang, Z. Zhang, Z. Wang, J. Deng, and D. G. Dorrell, "Chassis coordinated control for full X-by-wire vehicles-A review," *Chinese Journal of Mechanical Engineering*, vol. 34, no. 1, 42 pages, 2021.

[22] L. Zhang, Z. Wang, X. Ding, S. Li, and Z. Wang, "Fault-tolerant control for intelligent electrified vehicles against front wheel steering angle sensor faults during trajectory tracking," *IEEE Access*, vol. 9, Article ID 65174, 2021.

[23] B. Li, Y. Ouyang, Y. Zhang, T. Acarman, Q. Kong, and Z. Shao, "Optimal cooperative maneuver planning for multiple nonholonomic robots in a tiny environment via adaptive-scaling constrained optimization," *IEEE Robotics and Automation Letters*, vol. 6, no. 2, pp. 1511–1518, 2021.

[24] B. Li, Y. Zhang, Y. Feng, Y. Zhang, Y. Ge, and Z. Shao, "Balancing computation speed and quality: a decentralized motion planning method for cooperative lane changes of connected and automated vehicles," *IEEE Transactions on Intelligent Vehicles*, vol. 3, no. 3, pp. 340–350, 2018.

[25] B. Li, Y. M. Zhang, and Y. M. Ge, "Optimal control-based online motion planning for cooperative lane change motion plannings of connected and automated vehicles," in *Proceedings of the 2017 IEEE/RSJ International Conference on Intelligent Robots and Systems (IROS)*, pp. 3689–3694, Vancouver, BC, Canada, September 2017.

[26] Y. Liu and J. Jiang, "Optimum path-tracking control for inverse problem of vehicle handling dynamics," *Journal of Mechanical Science and Technology*, vol. 30, no. 8, pp. 3433–3440, 2016.